scientific reports

Check for updates

OPEN

A generalized SEIRW-VN framework for modeling infectious disease dynamics

Abdoulaye Sow[1]✉, Cherif Diallo[1] & Hocine Cherifi[2]

Understanding how infectious diseases spread requires models that integrate both human contact structure and environmental factors. We propose SEIRW-VN, a generalized epidemic framework that combines network heterogeneity, indirect transmission via environmental reservoirs, and vaccination. Using COVID-19 data from several European countries, the model outperforms classical homogeneous approaches, capturing more realistic epidemic peaks and timing. Our simulations reveal that highly connected individuals disproportionately sustain outbreaks, while environmental transmission can account for up to one quarter of infections, prolonging epidemic duration. Intervention analysis shows that non-pharmaceutical measures delay peaks and vaccination reduces long-term incidence, but only their combination yields strong synergistic effects, lowering both peak size and overall burden. These findings highlight the importance of integrating contact structure, environmental persistence, and vaccination into epidemic models to design robust and effective public health strategies.

Emerging and re-emerging infectious diseases remain a major concern for global health. Past outbreaks of influenza, dengue, and Zika have illustrated how quickly pathogens can spread and disrupt societies[1,2]. More recent epidemics of monkeypox, Ebola, cholera, and COVID-19 have further underlined the urgent need for effective prevention and control strategies[3–5]. A detailed understanding of transmission pathways is therefore essential to mitigate the impact of such crises[6].

Mathematical models are central to this effort. Classical compartmental frameworks such as the Susceptible–Infected–Recovered (SIR) and Susceptible–Exposed–Infected–Recovered (SEIR) models provide a foundation for analyzing epidemic dynamics and remain valuable despite their simplicity[4,7]. Over time, these models have been extended to incorporate heterogeneous contact patterns, human mobility, and pathogen persistence in the environment[8,9]. More recently, multilayer networks and higher-order interactions have been developed to capture population structure and collective behavior with greater accuracy[10–12]. Agent-based models (ABMs) offer a complementary perspective by explicitly simulating individuals and their interactions, and have been widely applied to evaluate interventions ranging from hospital infection control to vaccination strategies[13–17]. However, their computational cost and limited analytical tractability often restrict their use in large-scale comparative studies.

Despite these advances, few frameworks simultaneously account for direct person-to-person transmission, indirect transmission through contaminated environments, and the mitigating role of vaccination in structured populations. Such integration is particularly relevant for pathogens with multiple transmission routes, including cholera, Lassa fever, and SARS-CoV-2[6,18]. Previous work has typically focused on network heterogeneity[19,20] or environmental transmission[6,18], but rarely on both within a tractable mathematical framework.

Here we introduce the SEIRW-VN model, which extends the classical SEIR scheme by incorporating environmental transmission (W), vaccination dynamics (V), and contact heterogeneity through a heterogeneous mean-field network approach (N). This integrated formulation captures how network connectivity, vaccination coverage, and environmental contamination interact to shape epidemic trajectories. We empirically validate the model using data from the first wave of COVID-19 in Europe, where reliable datasets are available. Extension to other pathogens such as cholera, Lassa fever, or Zika is left as future work, requiring pathogen-specific parameterization and validation.

The structure of this article is as follows: Section Materials and methods details the SEIRW-VN model, its assumptions, and the calibration procedure using COVID-19 datasets. Section Results reports the main outcomes, including model comparison, the role of network heterogeneity, the evaluation of intervention strategies, and the contribution of environmental transmission. Section Discussion interprets these results in

[1]Department of Computer Science, Algebra Laboratory for Cryptography, Codes and Applications, Gaston Berger University, Saint-Louis, Senegal. [2]Department of Computer Science, ICB, UMR 6303 CNRS, Université Bourgogne Europe France, Dijon, France. ✉email: sow.abdoulaye6@ugb.edu.sn

the context of related studies and highlights their implications. Finally, Section Conclusion summarizes the key contributions and provides perspectives for future research on epidemic preparedness and response.

Materials and methods

Model structure under heterogeneous mean-field approximation

The SEIRW-VN model extends the classical SEIR framework by integrating three key components. First, an environmental compartment (W) is included to account for indirect transmission through viral persistence. Second, asymptomatic transmission and vaccination are explicitly represented, allowing the model to capture both hidden spreaders and preventive measures. Third, contact heterogeneity is incorporated using a heterogeneous mean-field (HMF) approximation of a scale-free network. In this setting, individuals are grouped by degree, and highly connected nodes play a disproportionate role in transmission dynamics. This representation provides a more realistic description of scenarios where certain individuals or locations act as hubs that accelerate the spread of infection.

Rationale for the methodological choice

Traditional compartmental models with homogeneous mixing tend to oversimplify epidemic dynamics by ignoring variation in individual contact patterns. Network-based approaches highlight the impact of community clustering and highly connected individuals, who can disproportionately drive transmission. At the same time, environmental transmission, documented for several pathogens, sustains epidemics by acting as a reservoir of infection. Our model integrates these dimensions direct and indirect transmission, contact heterogeneity, and vaccination into a unified framework. This formulation provides a more realistic basis for analyzing epidemic dynamics and for evaluating the effectiveness of public health interventions across a wide range of infectious diseases

Model framework and assumptions

In order to account for contact heterogeneity, we extend a deterministic SEIR-W model using the heterogeneous mean field (HMF) approximation applied The contact network was generated using the Barabási-Albert model with minimal degree $m = 8$, yielding an average degree $\langle k \rangle \approx 16$, consistent with empirical social contact data[21]. To assess the robustness of our results to network connectivity, we conducted a comprehensive sensitivity analysis by varying the minimal degree parameter m across values $\{1, 3, 5, 8, 10\}$.

As shown in Fig. 1, increasing m leads to higher average connectivity and consequently to a higher transmission potential, with R_0 increasing monotonically as m grows. Despite this quantitative variation, all qualitative findings regarding superspreader dynamics and intervention effectiveness remain robust across the tested parameter range. In this framework, individuals are grouped into degree classes based on the number k of contacts they have within the network. For each degree class k, we define the following compartments: $S_k(t)$ for susceptible individuals, $E_k(t)$ for exposed but not yet infectious individuals, $I_{A,k}(t)$ for asymptomatic infectious individuals, $I_{S,k}(t)$ for symptomatic infectious individuals, $R_k(t)$ for recovered individuals, and $V_k(t)$ for vaccinated individuals. In addition, we denote by $W(t)$ the environmental viral load, which is shared across the entire population and acts as an additional transmission pathway.

The model is based on the following assumptions. First, the total population size N_{total} is constant and its degree distribution follows the scale-free law $P(k) \sim k^{-3}$. Secondly, transmission of infection can occur either directly through network contacts or indirectly through the environmental compartment W.Thirdly, vaccination begins at a certain time t_v and is characterised by a maximum vaccination rate φ_0 and an efficacy parameter q. Fourthly, asymptomatic and symptomatic individuals contribute differently to direct transmission and the spread of the virus in the environment. Finally, the environmental reservoir W receives inputs from infectious individuals and undergoes natural degradation at a rate μ_W.

Under these assumptions, the epidemic dynamics for each degree class k are described by the following system of differential equations:

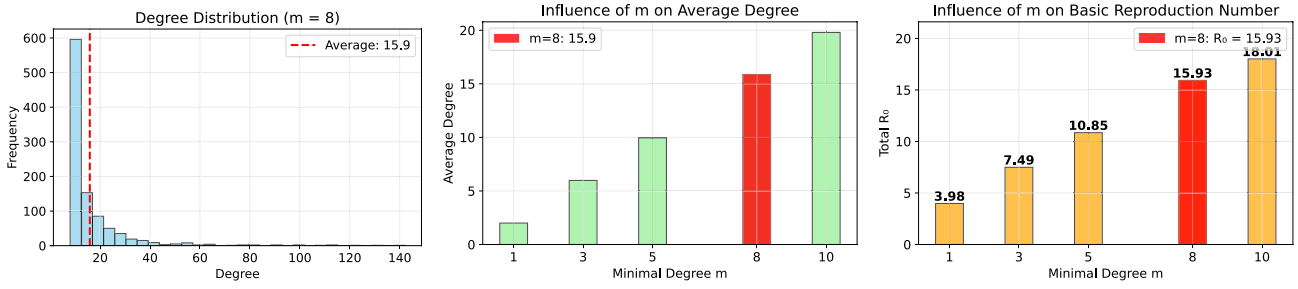


Fig. 1. Sensitivity analysis of network connectivity. (**A**) Degree distribution for the chosen parameter $m = 8$. (**B**) Influence of minimal degree m on average network degree. (**C**) Impact of m on the basic reproduction number R_0, showing increased transmission potential with higher connectivity.

$$
\begin{aligned}
\dot{S}_k &= -\lambda_k(t) S_k - \varphi(t) q S_k, \\
\dot{E}_k &= \lambda_k(t) S_k - \kappa E_k, \\
\dot{I}_{A,k} &= p_{\text{asym}} \kappa E_k - \omega I_{A,k} - \gamma_A I_{A,k}, \\
\dot{I}_{S,k} &= (1 - p_{\text{asym}}) \kappa E_k + \omega I_{A,k} - \nu I_{S,k}, \\
\dot{R}_k &= \nu I_{S,k} + \gamma_A I_{A,k}, \\
\dot{V}_k &= \varphi(t) q S_k.
\end{aligned}
$$

The environmental compartment evolves according to

$$
\dot{W} = \frac{1}{N_{total}} \sum_k P(k) \left(\sigma_A I_{A,k} + \sigma_S I_{S,k} \right) - \mu_W W,
$$

where σ_A and σ_S denote the respective rates of viral shedding by asymptomatic and symptomatic individuals.

The probability that a susceptible individual of degree k acquires infection at time t is defined as the force of infection $\lambda_k(t)$. In its general form, it depends on the contact matrix $C_{kk'}$ between classes k and k':

$$
\lambda_k(t) \;=\; \sum_{k'} C_{kk'}(t) \, \frac{\beta_A I_{A,k'}(t) + \beta_S I_{S,k'}(t)}{N_{k'}} + \beta_W W(t).
$$

The contact matrix $C_{kk'}$ represents the expected number of contacts between individuals belonging to degree classes k and k'. Each element quantifies how frequently a person with k connections interacts with individuals having k' connections. In the heterogeneous mean-field (HMF) framework, this matrix provides a statistical description of the network structure without explicitly simulating each individual. Assuming an uncorrelated scale-free network, as generated by the Barabási–Albert model, the probability that a link connects two degree classes is proportional to $kk'/(N_{total}\langle k \rangle)$. Accordingly, the contact matrix can be written as $C_{kk'} \propto kk'/(N_{total}\langle k \rangle)$, which simplifies the force of infection for degree class k to

$$
\lambda_k(t) = k \, \Theta(t) + \beta_W W(t),
$$

where

$$
\Theta(t) = \frac{1}{\langle k \rangle} \sum_{k'} P(k') \, k' \, \frac{\beta_A I_{A,k'}(t) + \beta_S I_{S,k'}(t)}{N_{k'}}.
$$

This formulation highlights the disproportionate influence of highly connected nodes ("hubs") in sustaining transmission while keeping the model analytically tractable for calibration and sensitivity analysis.

Here, β_W denotes the environmental transmission rate, $\langle k \rangle$ the average degree of the network, and $N_{k'}$ the population size of degree class k'.

The vaccination rate $\varphi(t)$ is modeled as a step function:

$$
\varphi(t) = \begin{cases} 0, & t < t_v, \\ \varphi_0, & t \geq t_v, \end{cases}
$$

The structure of the model is illustrated in Fig. 2. The parameters of the model and their definitions are summarized in Table 1.

Basic reproduction number

To quantify the epidemic potential of the system, we linearize the model at the disease-free equilibrium and apply the next-generation method. The resulting basic reproduction number R_0 can be decomposed into two additive contributions corresponding to direct transmission through the network and indirect transmission via the environment:

$$
R_0 \;=\; R_0^{(\text{dir})} \;+\; R_0^{(\text{env})}.
$$

The first component, $R_0^{(\text{dir})}$, represents the average number of secondary infections generated by a single infectious individual through direct contacts in the heterogeneous network. It is given by

$$
R_0^{(\text{dir})} \;=\; \frac{\langle k^2 \rangle}{\langle k \rangle} \; \mathscr{T}_{\text{dir}},
$$

where

$$
\mathscr{T}_{\text{dir}} = p_{\text{asym}} \, \beta_A \, D_A + (1 - p_{\text{asym}}) \, \beta_S \, D_S.
$$

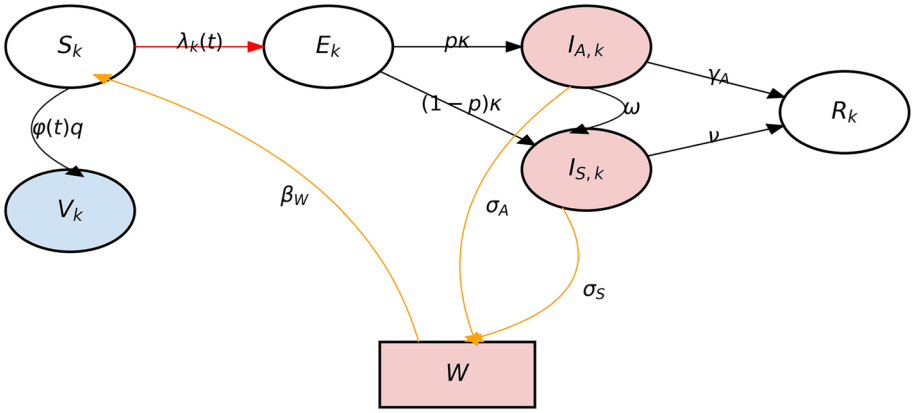


Fig. 2. Compartmental diagram of the SEIRW-VN model. Red arrows indicate direct person-to-person transmission, orange arrows represent indirect transmission through the environment, and red circles highlight the infectious compartments responsible for disease spread.

Parameter	Symbol	Value (range)	Source/Notes
Direct transmission rate (asymptomatic)	β_A	0.15–0.35 day^{-1}	Estimated
Direct transmission rate (symptomatic)	β_S	0.25–0.50 day^{-1}	Estimated
Environmental transmission rate	β_W	0.02–0.08 day^{-1}	Estimated
Environmental decay rate	μ_W	0.6 day^{-1}	18,22
Incubation rate	κ	$1/7\text{day}^{-1}$	23
Asymptomatic recovery rate	γ_A	0.0526 day^{-1}	24
Proportion asymptomatic	p_{asym}	0.2072	Estimated
Symptomatic recovery rate	ν	0.1 day^{-1}	24
Vaccination rate	φ_0	0.4	25
Vaccine efficacy	q	0.7(0.6–0.8)	26
Average network degree	$\langle k \rangle$	10–20	21
viral shedding rates for asymptomatic	σ_A	0.24 day^{-1}	Estimated
viral shedding rates for symptomatic	σ_S	0.39 day^{-1}	Estimated
Rate at which asymptomatic individuals become symptomatic	ω	0.13978 day^{-1}	27

Table 1. Key parameters of the SEIRW-VN model with sources and calibration notes.

In this expression, D_A and D_S denote the mean infectious durations of asymptomatic and symptomatic individuals, respectively. Asymptomatic individuals may either recover at rate γ_A or progress to the symptomatic stage at rate ω, which leads to

$$D_A = \frac{1}{\omega + \gamma_A}.$$

Symptomatic individuals exit the infectious compartment at rate ν, resulting in

$$D_S = \frac{1}{\nu}.$$

The second component, $R_0^{(\text{env})}$, corresponds to infections caused through the environmental route. It is expressed as

$$R_0^{(\text{env})} = \beta_W \left(p_{\text{asym}} \frac{\sigma_A D_A}{\mu_W} + (1 - p_{\text{asym}}) \frac{\sigma_S D_S}{\mu_W} \right).$$

This term reflects the combined effect of environmental transmission rate, viral shedding by infectious individuals, and the persistence of the pathogen in the environment.

Overall, these results highlight the dual nature of transmission in the SEIRW-VN model under heterogeneous mixing. The factor $\langle k^2 \rangle / \langle k \rangle$ emphasizes the amplifying role of degree heterogeneity in scale-free networks, where highly connected individuals contribute disproportionately to epidemic spread. At the same time, the environmental pathway provides an indirect mechanism that can sustain transmission even when direct contacts are limited.

Calibration protocol: application to COVID-19

To illustrate the SEIRW-VN framework, we analyzed the first wave of COVID-19 in Europe using daily case counts from Spain, Belgium, Switzerland, and Italy, obtained from the European Centre for Disease Prevention and Control (ECDC)[28]. These harmonized datasets provide a consistent reference for cross-country comparison.

Calibration focused on key epidemiological parameters: transmission rates for asymptomatic and symptomatic individuals (β_A, β_S), the environmental transmission rate (β_W), viral shedding rates (σ_a, σ_s), vaccination rate (q) and the proportion of asymptomatic infections (p_{asym}). Together, these govern the relative contributions of direct and environmental pathways.

Parameters were inferred using Approximate Bayesian Computation (ABC) with the rejection algorithm[29]. Candidate sets were sampled from uniform priors (Table 1) and used to generate epidemic trajectories stratified by network degree. Simulated and observed incidence were compared using normalized root mean square error (NRMSE), and the top 1% of simulations were retained to approximate the posterior distribution. Repeated runs ensured robust exploration of parameter space.

Model fit was evaluated by Root Mean Square Error (RMSE), with uncertainty quantified by bootstrap confidence intervals around fitted trajectories. Out-of-sample validation was performed by training on an initial period and testing predictions on later data, using RMSE and Mean Absolute Error (MAE) as complementary metrics.

Although the SEIRW-VN model is deterministic for a given set of parameters, uncertainty arises from two sources: parameter estimation and variability in network structure. The 95% confidence intervals shown in Figs. 6, 7, 11, and 12 were obtained by propagating these sources of uncertainty. Parameter values were drawn from their posterior distributions obtained through the Approximate Bayesian Computation (ABC) procedure. For each accepted parameter set, the model was simulated 500 times on independent realizations of the scale-free network with the same degree distribution. The shaded regions represent the 2.5th to 97.5th percentiles of the resulting ensemble of trajectories. In the "no-control" scenario, the intervals reflect only parameter and network uncertainty, while in intervention scenarios they also include random modulation of contact reduction to capture heterogeneous compliance with NPIs and vaccination rollout. This ensemble approach provides a probabilistic envelope around the deterministic model, enhancing both interpretability and reproducibility.

This calibration yields a data-driven representation of COVID-19 dynamics in each country. The next section presents simulation results, including epidemic curves, uncertainty intervals, and the impact of intervention strategies.

Simulation scenarios

To explore the impact of different interventions and contextual factors on epidemic dynamics, we consider several sets of simulation scenarios. These scenarios distinguish between the pre-vaccination phase, the post-vaccination phase with different rollout speeds, and the role of environmental transmission. This structure allows us to assess separately and jointly the effects of non-pharmaceutical interventions, vaccination strategies, and environmental factors.

Pre-vaccination phase

Three distinct scenarios are considered to evaluate the effect of non-pharmaceutical interventions before the introduction of vaccines.

Scenario 1: Full release (baseline) No control is applied and the mobility matrix C_{ij} remains unchanged. This reference case corresponds to the absence of distancing measures or contact reduction.

Scenario 2: Partial lockdown Interpersonal contacts are moderately reduced by proportionally attenuating the coefficients of the matrix C_{ij}. This scenario reflects partial restrictive measures, such as limits on gatherings or reduced mobility.

Scenario 3: Alternating lockdown Contacts are strongly and intermittently reduced through a temporal modulation of the matrix C_{ij}. This scenario illustrates a strategy aimed at slowing transmission while maintaining some social and economic activity.

Post-vaccination phase

The post-vaccination phase begins at day $t_v = 30$, earlier than in the baseline scenario in order to emphasize the importance of timely rollout. Three vaccination rollout speeds are considered, defined by the maximal vaccination rate φ_0:

$\varphi_0 = 0.1$
$\varphi_0 = 0.2$
$\varphi_0 = 0.5$.

In addition, combined scenarios are introduced, associating vaccination with the non-pharmaceutical interventions (NPIs) defined in the pre-vaccination phase. These combinations explore the joint effect of reduced contacts and increasing vaccine coverage.

Country	SEIRW	SEIRW-VN	ΔAIC
Belgium	1523.4	1462.7	60.7
Italy	1687.9	1622.2	65.7
Spain	1456.8	1411.0	45.8
Switzerland	1388.5	1379.7	8.8

Table 2. Comparison of AIC values between SEIRW and SEIRW-VN. A positive ΔAIC means SEIRW-VN performs better.

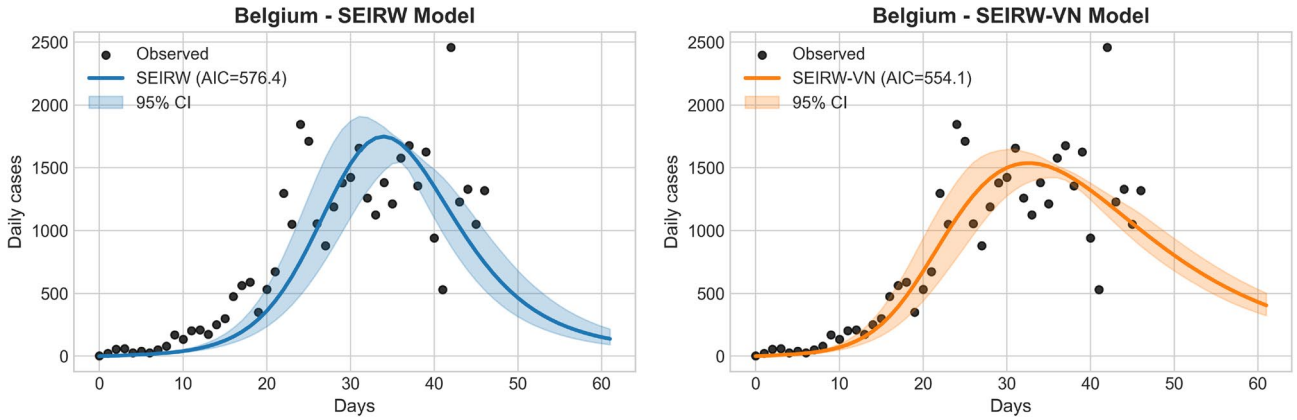


Fig. 3. Belgium: model fits with SEIRW (left) and SEIRW-VN (right).

Environmental scenarios

In addition to the pre- and post-vaccination phases, we also consider environmental scenarios to assess the impact of indirect transmission via the environmental reservoir (W). Two main factors are explored: weak vs. strong environmental transmission, obtained by varying the parameter β_W, and short vs. long persistence, controlled by the viral decay parameter μ_W.

These scenarios characterize the effect of environmental conditions on epidemic dynamics, explicitly accounting for the contribution of the compartment W within the SEIRW-VN model.

Results

This section presents the main results obtained from simulations of the hybrid SEIRW-VN model coupled with network framework. The objective is to assess the validity of the proposed modeling approach and to analyze the impact of different intervention strategies on epidemic dynamics. The results are organized into several parts: model validation, the effect of structural heterogeneity, the impact of non-pharmaceutical interventions, vaccination strategies, the role of environmental transmission, and global sensitivity analyses.

Comparison SEIRW vs SEIRW-VN

The comparison between SEIRW and SEIRW-VN is based on the Akaike Information Criterion (AIC). A lower AIC means a better fit while accounting for model complexity. The results for Belgium, Italy, Spain and Switzerland (Table 2) show that the SEIRW-VN model always gives lower AIC values than SEIRW. The differences range from 8.8 (Switzerland) to 65.7 (Italy), which is strong evidence in favor of the extended model.

Figures 3, 4, 5 and 6 show these results for each country. In all cases, SEIRW-VN fits the epidemic curves better and produces confidence intervals that agree more closely with the data.

These results show that adding a network dimension in SEIRW-VN makes it possible to capture contact heterogeneity and real COVID-19 spread more accurately. SEIRW-VN is therefore more robust and realistic than SEIRW for modeling epidemic dynamics.

Impact of structural heterogeneity

In this section, we study how contact heterogeneity affects epidemic spread. We first compare a homogeneous model, with perfect mixing, to a network model that reflects social structure. Then, we look at the role of highly connected individuals, called superspreaders, and the effect of infection duration.

Network vs homogeneous comparison

The homogeneous model produces a smooth and symmetric curve. It overestimates the peak by about 30% and predicts it 10 to 15 days too early. The network model shows a later peak, a slower decline, and larger variability. This variability is not visible with the homogeneous approach (Fig. 7).

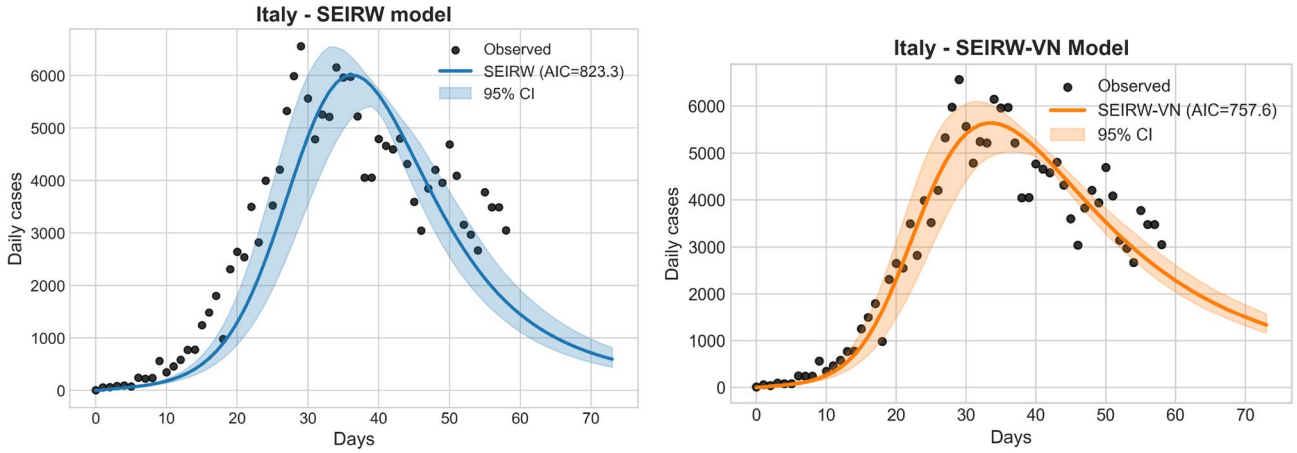


Fig. 4. Italy: model fits with SEIRW (left) and SEIRW-VN (right).

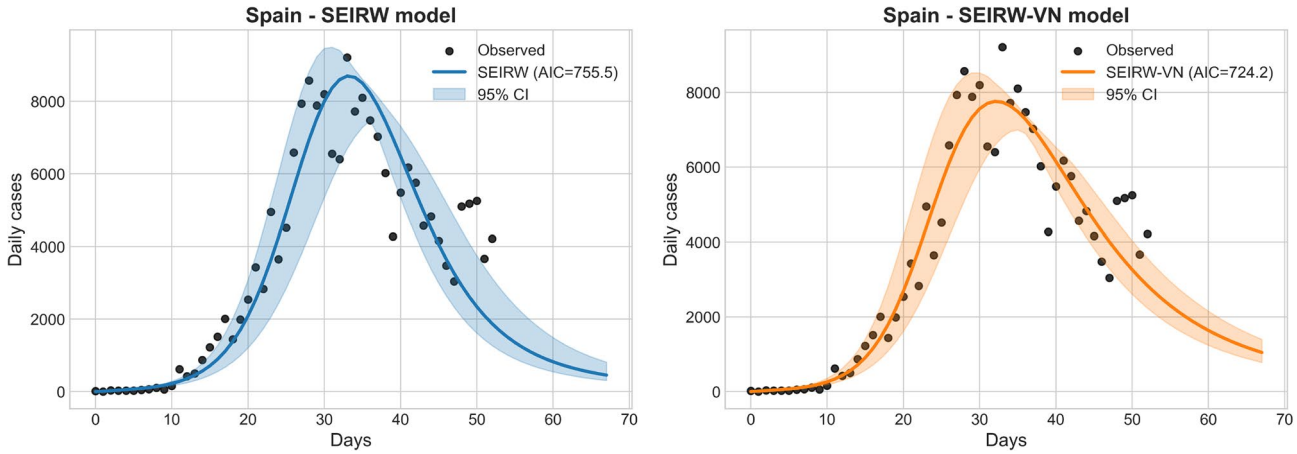


Fig. 5. Spain: model fits with SEIRW (left) and SEIRW-VN (right).

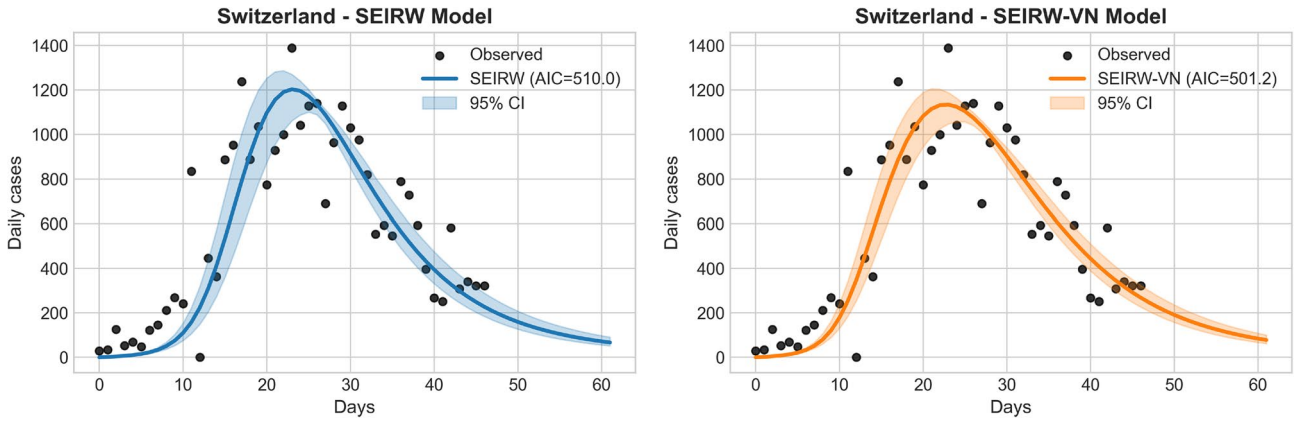


Fig. 6. Switzerland: model fits with SEIRW (left) and SEIRW-VN (right).

Superspreaders and connectivity

Beyond the general comparison between homogeneous and network approaches, it is essential to examine the impact of individual heterogeneity on the spread of the epidemic. This section focuses in particular on the role of superspreaders, i.e. highly connected individuals who contribute disproportionately to transmission.

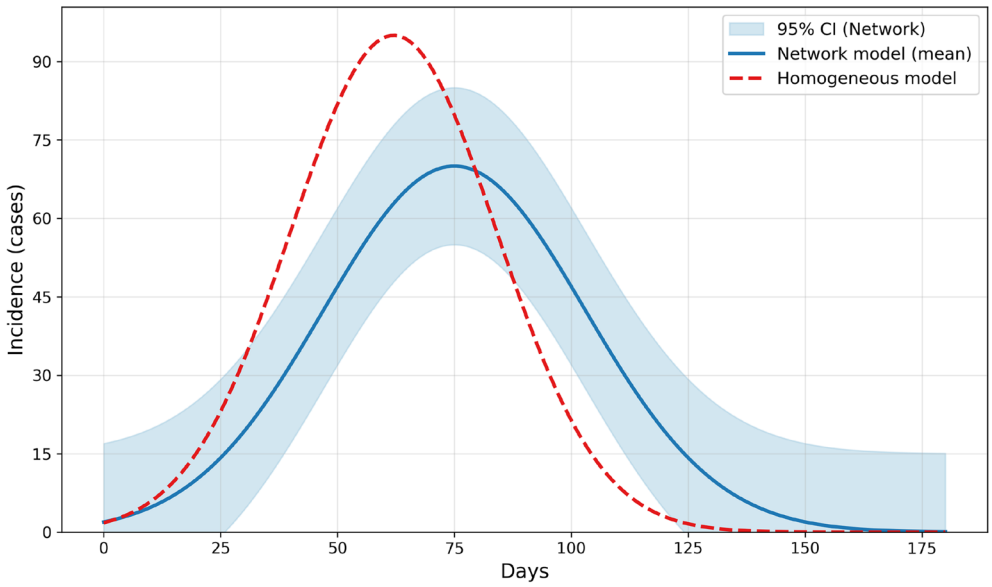
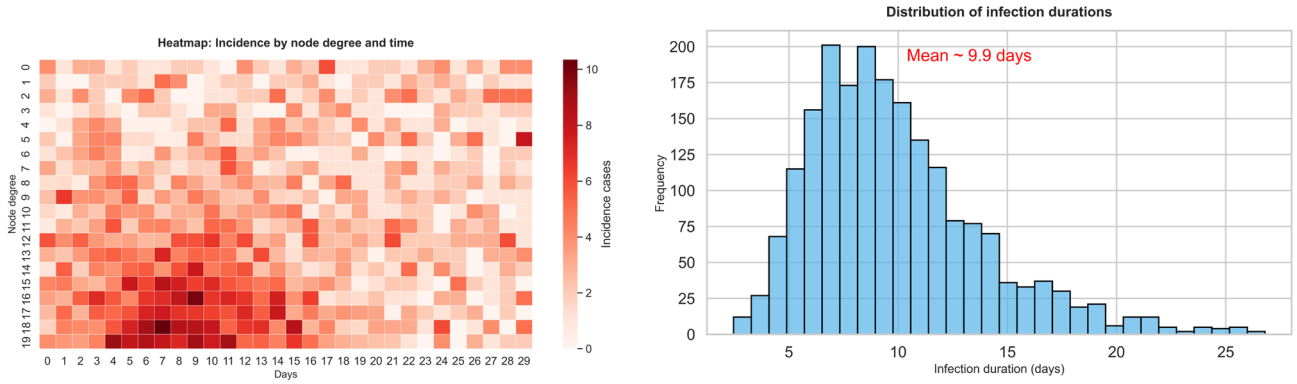


Fig. 7. Comparison between homogeneous model (red) and network model (blue). Shaded areas are 95% confidence intervals.



(a) Incidence by node degree

(b) Infection duration

Fig. 8. (**a**) Heatmap of incidence by degree and time. (**b**) Distribution of infection durations.

The heatmap (Fig. 8a) shows that these nodes have much higher incidence. Transmission accelerates in the first days. The histogram (Fig. 8b) shows a mean infection duration of about 9.9 days. This mean duration is consistent with the cure rate parameters in Table 1 and a calibrated asymptomatic proportion of 20,7%. When long infections combine with high connectivity, the epidemic is stronger and lasts longer.

These results show that control strategies should target superspreaders and long infectious individuals. Targeted vaccination and reinforced testing are adapted strategies.

Effect of non-pharmaceutical interventions (NPIs)

We study the effect of NPIs on epidemic dynamics. The goal is to see how contact reduction changes the peak size, timing, and total incidence.

As shown in Fig. 9, without measures (full release), the peak is very high, around day 42 with about 78 cases per 1000. Semi-lockdown cuts the peak in half (about 39 cases per 1000, –50%) and delays it by about 16 days. Alternating lockdown reduces the peak further (about 23 cases per 1000, –70%) and delays it by about 30 days.

NPIs lower the effective contact rate, slowing transmission and spreading cases over time. Alternating lockdown acts as a buffer: it flattens the epidemic curve, reduces hospital pressure, and gives more time for vaccination or surveillance. The confidence bands confirm robust effects around the peak, though extreme trajectories remain possible, especially under full release. In the pre-vaccination phase, NPIs are therefore essential to reduce peaks and buy time for additional control measures.

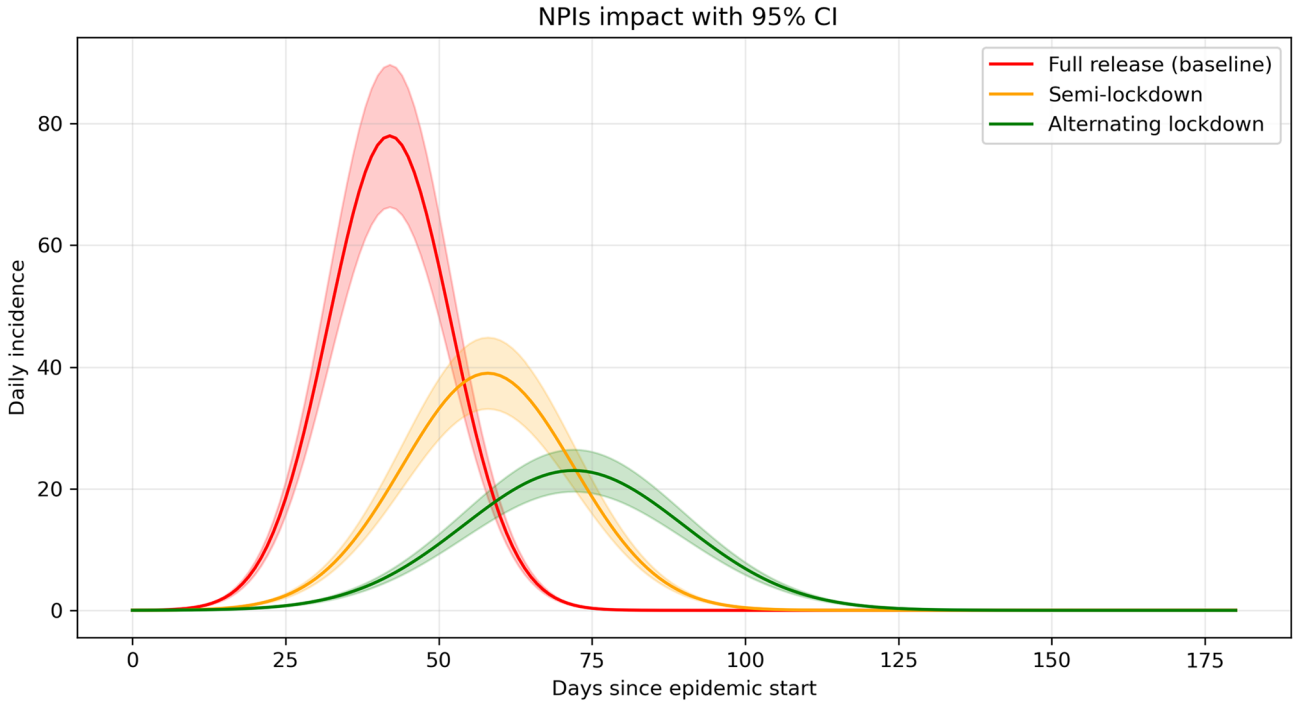


Fig. 9. Impact of NPIs on daily incidence (pre-vaccination phase). Mean curves and 95% CI from simulations for: full release (red), semi-lockdown (orange), and alternating lockdown (green).

Vaccination strategies

We now study the effect of vaccination strategies on epidemic dynamics, considering both vaccination speed and the role of NPIs.

As shown in Fig. 10, slow vaccination alone reduces the peak only slightly (about 70 cases per 1000 compared to 78 in the baseline), because immunity builds up gradually. In contrast, faster vaccination campaigns have a stronger impact, and when combined with NPIs, the effect is highly synergistic. For example, the combination of semi-lockdown and rapid vaccination lowers the peak to about 15 cases per 1000 (a reduction of nearly 80

This contrast highlights the different mechanisms: NPIs act immediately by reducing contacts, whereas vaccination requires time to achieve protection. As a result, a slow rollout may appear to have a similar impact to semi-lockdown in the long term, but the short-term benefits of NPIs are much stronger in practice. The synergy between rapid vaccination and NPIs produces the most robust reductions, lowering both the epidemic peak and the cumulative number of cases, while also reducing variability across simulations. If vaccination starts too late, after the peak, its impact on maximum incidence is limited, but it still contributes to reducing the epidemic size and duration.

Targeting strategy

We compare two approaches: random vaccination and targeted vaccination of the most connected nodes (hubs).

Figure 11 shows that targeting hubs is more effective than random vaccination. It lowers the total epidemic size and speeds up the decline. This highlights that vaccination strategies are more efficient when they take into account the heterogeneity of social contacts.

Comparative analysis of intervention scenarios

This section compares the simulated scenarios. We focus on three dimensions: cumulative incidence, epidemic peaks, and summary indicators. The goal is to show the overall impact of NPIs, vaccination, and combined strategies.

Cumulative incidence by scenario

Figure 12 shows that the cumulative incidence without control reaches approximately 2800 cases. This incidence is reduced to 1800 cases by non-pharmaceutical interventions (NPIs), and to 2200 cases with a slow vaccination campaign. The combination of NPIs and a fast vaccination strategy lowers it further to just 800 cases, resulting in far fewer hospitalizations, deaths, and reduced social impact.

Distribution of epidemic peaks

Boxplots show that NPIs with fast vaccination reduce both the median peak and its variability see (Fig. 13). This lowers the chance of extreme events and health system overload.

The comparative analysis highlights several important findings. First, NPIs reduce the height of the epidemic peak and delay its timing, providing critical time for the health system to adapt and preventing immediate

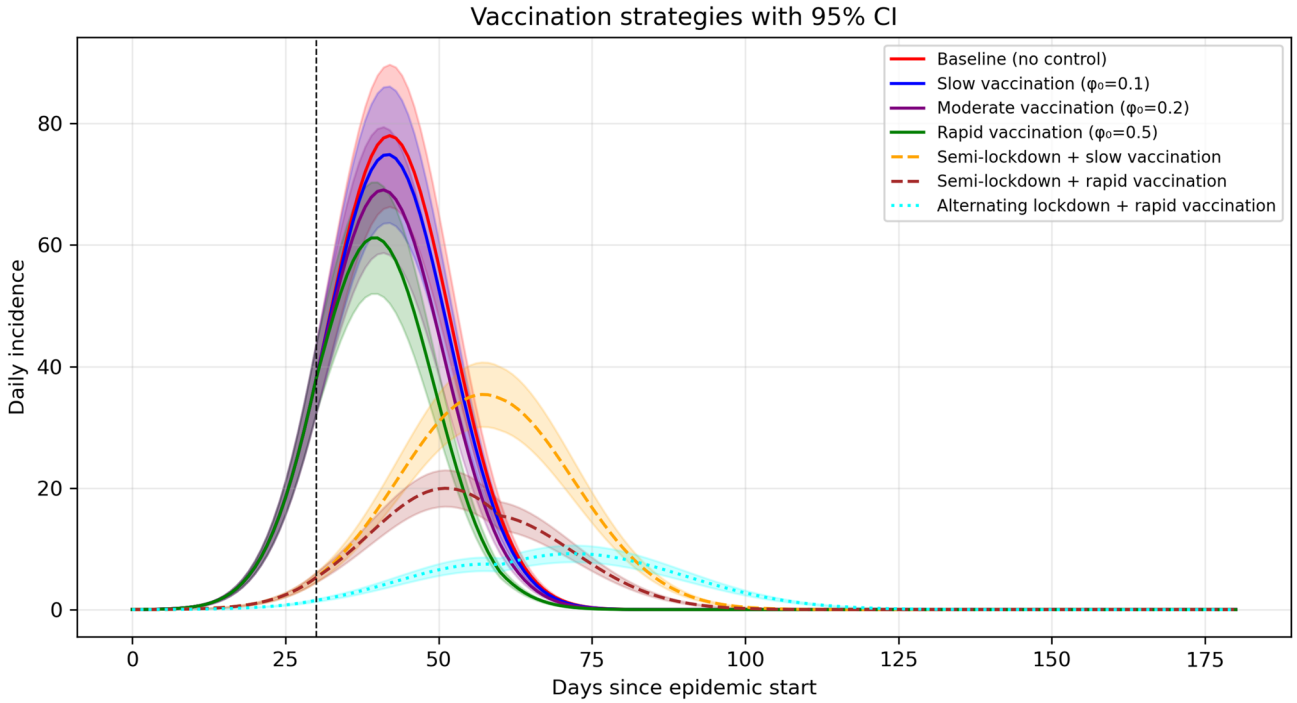


Fig. 10. Impact of vaccination strategies on daily incidence. Curves show the effect of vaccination speed (slow, moderate, rapid) and the combination with NPIs. Shaded areas indicate 95% confidence intervals.

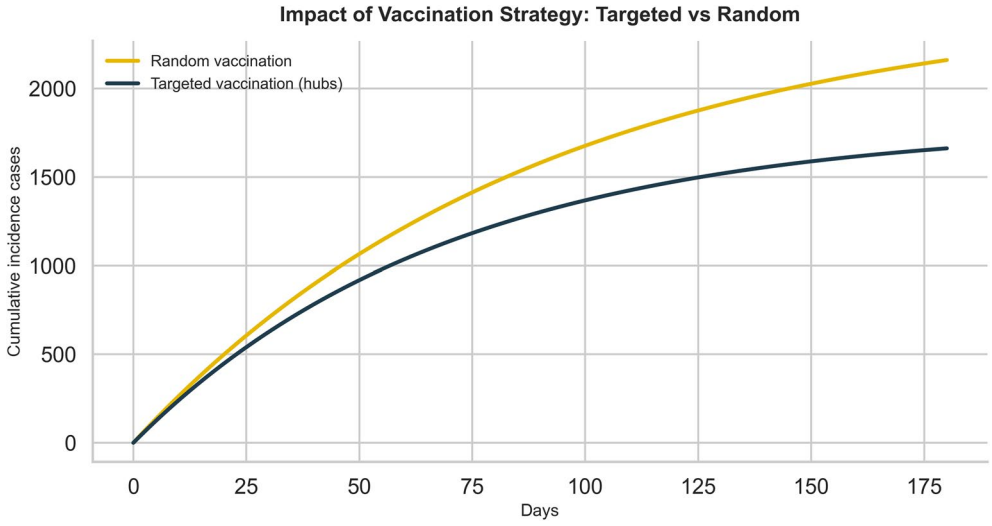


Fig. 11. Impact of random vaccination and targeted vaccination (hubs) on cumulative incidence.

overload. Second, vaccination shows a strong effect only when rollout is fast. A slow deployment reduces cases but remains insufficient to control the epidemic. The combination of NPIs with fast vaccination produces the strongest impact, lowering both cumulative incidence and peak size while also reducing variability across simulations. This robustness is important, as it minimizes the probability of extreme trajectories that could challenge hospital capacity. Third, the contact structure plays a decisive role. Models that account for network heterogeneity provide different estimates than homogeneous-mixing models, especially in terms of peak magnitude and timing. These results confirm that realistic network effects must be included to design efficient intervention strategies.

Temporal evolution of the effective reproduction number (R_t)

The effective reproduction number is obtained by weighting the basic reproduction number R_0 with the proportion of susceptibles at time t:

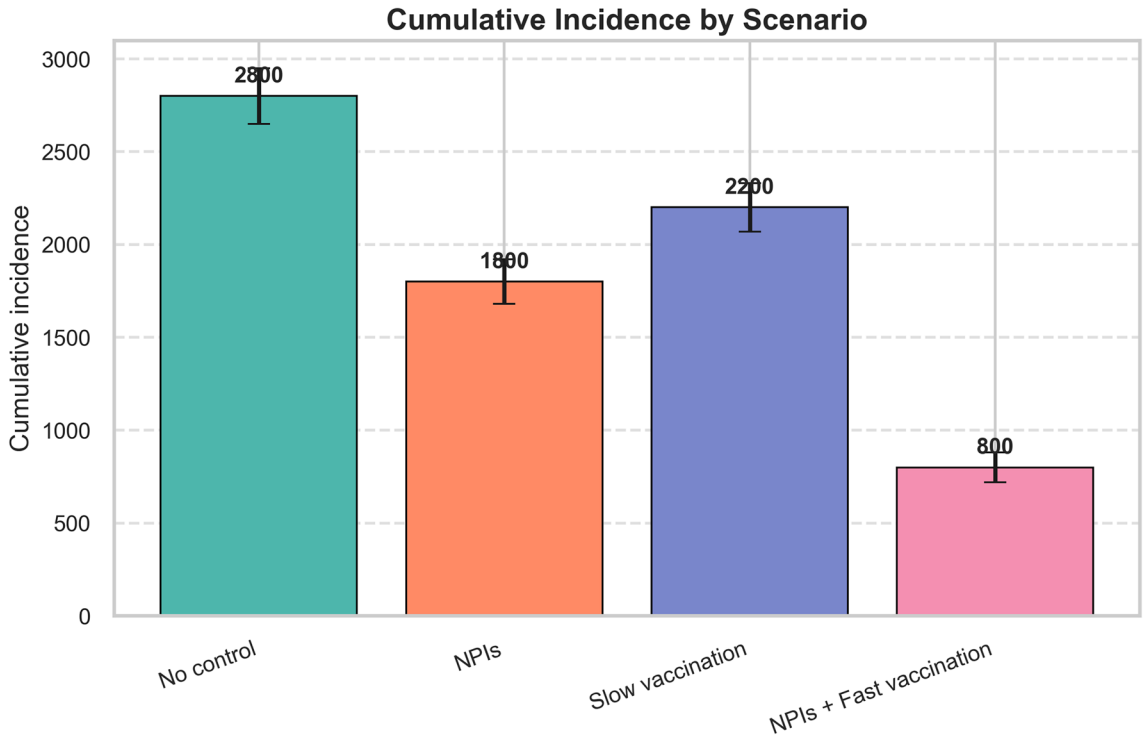


Fig. 12. Cumulative incidence by scenario.

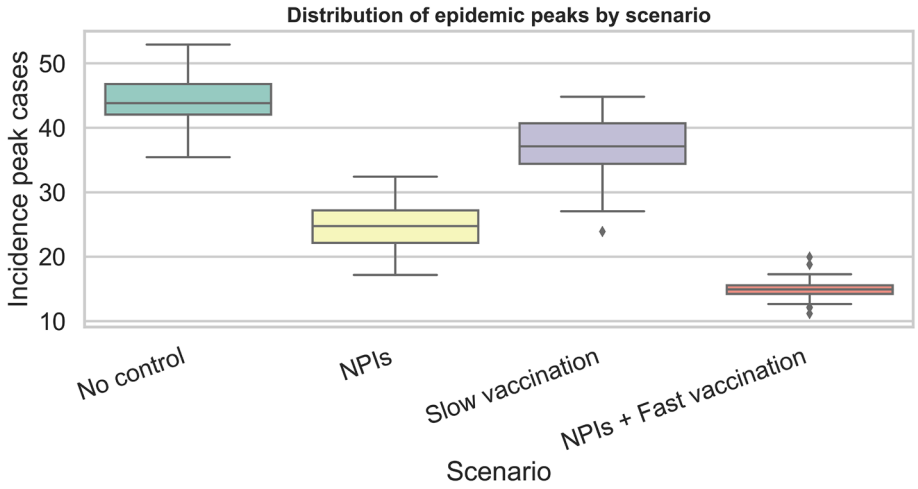


Fig. 13. Distribution of epidemic peaks by scenario.

$$R_t = R_0 \cdot \frac{S(t)}{N_{total}}. \tag{1}$$

In the SEIRW-VN framework, R_0 decomposes into two additive parts: direct transmission through the contact network and indirect transmission via the environment,

$$R_0 = R_0^{(\mathrm{dir})} + R_0^{(\mathrm{env})}. \tag{2}$$

Thus, the effective reproduction number is finally expressed as

$$R_t = \left[\frac{\langle k^2 \rangle}{\langle k \rangle} \left(p_{\mathrm{asym}}\, \beta_A D_A + (1 - p_{\mathrm{asym}})\, \beta_S D_S \right) + \beta_W \left(\frac{p_{\mathrm{asym}}\, \sigma_A D_A}{\mu_W} + \frac{(1 - p_{\mathrm{asym}})\, \sigma_S D_S}{\mu_W} \right) \right] \cdot \frac{S(t)}{N_{total}}. \tag{3}$$

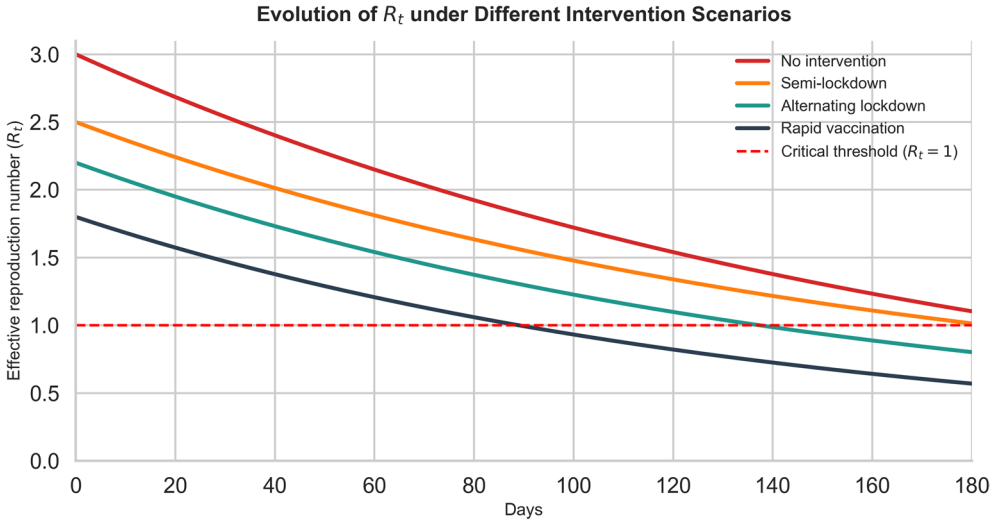


Fig. 14. Evolution of the effective reproduction number (R_t) under different scenarios. The dashed red line marks the critical threshold $R_t = 1$.

Metric	$\langle k \rangle = 10$	$\langle k \rangle = 15$	$\langle k \rangle = 20$	Change (%)
Peak incidence (cases/day)	168.3	218.9	245.4	+45.8%
Peak timing (day)	58	48	43	−25.9%
Cumulative incidence (cases)	2850	3450	3780	+32.7%
Maximum R_t	2.84	3.62	4.21	+48.2%
Time $R_t > 1$ (days)	112	124	136	+21.4%

Table 3. Sensitivity analysis results for network degree variation.

The effective reproduction number R_t is a key indicator of epidemic dynamics, as it marks the transition between growth and decline when crossing the critical threshold of 1. Figure 14 illustrates how R_t changes over time under different intervention scenarios.

Without intervention, R_t remains well above 1 throughout the 180-day horizon, reflecting sustained transmission. Semi-lockdown slows the decline but only approaches the threshold at the very end of the simulation. Alternating lockdown performs better, reducing transmission to below 1 around day 140. By contrast, rapid vaccination proves the most effective, crossing the threshold near day 90 and maintaining values below 1 thereafter. Overall, Fig. 14 demonstrates that vaccination speed is decisive for shortening the high-transmission phase and mitigating the risk of healthcare system overload.

Sensitivity to network degree

To further assess the robustness of the SEIRW-VN framework with respect to population connectivity, we performed a sensitivity analysis on the average network degree $\langle k \rangle$. Three representative values ($\langle k \rangle = 10, 15, 20$) were considered to reflect different contact intensities observed across European populations[21]. Higher values of $\langle k \rangle$ correspond to more connected societies, while lower values represent reduced interaction intensity.

Table 3 summarizes the corresponding numerical outcomes. As shown in both Fig. 15 and Table 3, increasing $\langle k \rangle$ from 10 to 20 leads to a ∼46% higher epidemic peak and advances its timing by about 15 days, while the qualitative epidemic trajectory remains stable.

Although the SEIRW–VN model remains robust to moderate variations in the average network degree, this analysis assumes a uniform $\langle k \rangle$ across the population. In reality, contact patterns are heterogeneous and may vary by age, social setting, or behavior. Future work should incorporate heterogeneous or dynamic contact structures to better capture real-world variability and assess how adaptive behaviors or clustered networks influence epidemic outcomes.

Environmental transmission

This section examines the role of the environmental compartment in epidemic dynamics. We consider three aspects: the evolution of viral load, its relative contribution to transmission, and the effect of key parameters (β_W and μ_W). Results show that indirect transmission acts as an epidemic memory, extending contagion beyond the infection peak.

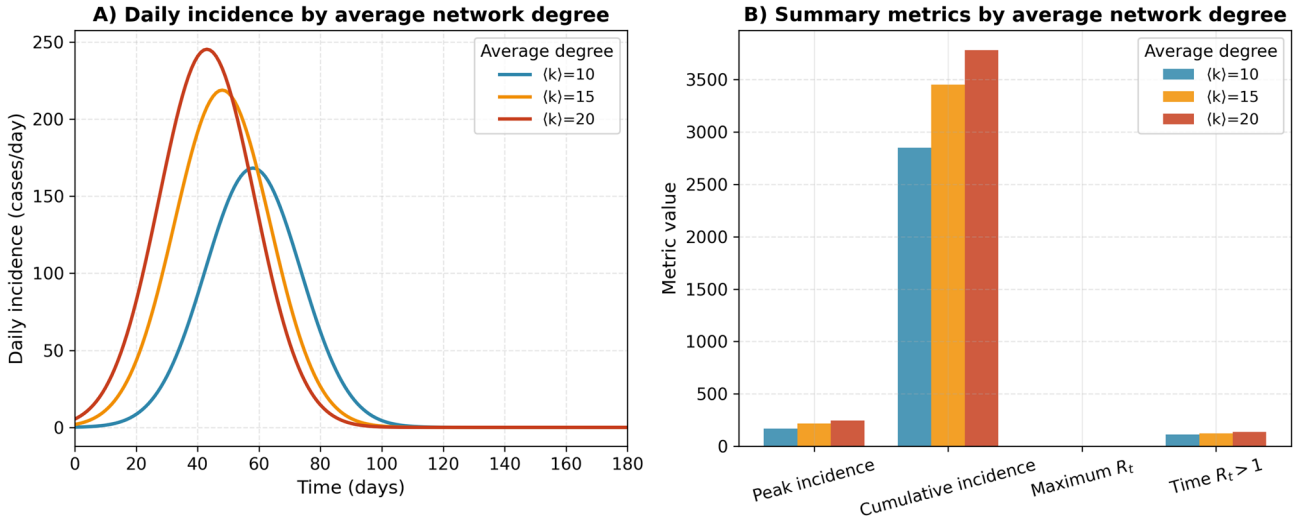


Fig. 15. Sensitivity of epidemic dynamics to average network degree. (**A**) Simulated daily incidence for three levels of mean connectivity ($\langle k \rangle = 10, 15, 20$), showing higher and earlier peaks with increased contact intensity. (**B**) Comparative summary metrics consistent with Table 3, confirming that moderate variations in $\langle k \rangle$ amplify transmission but preserve qualitative epidemic patterns.

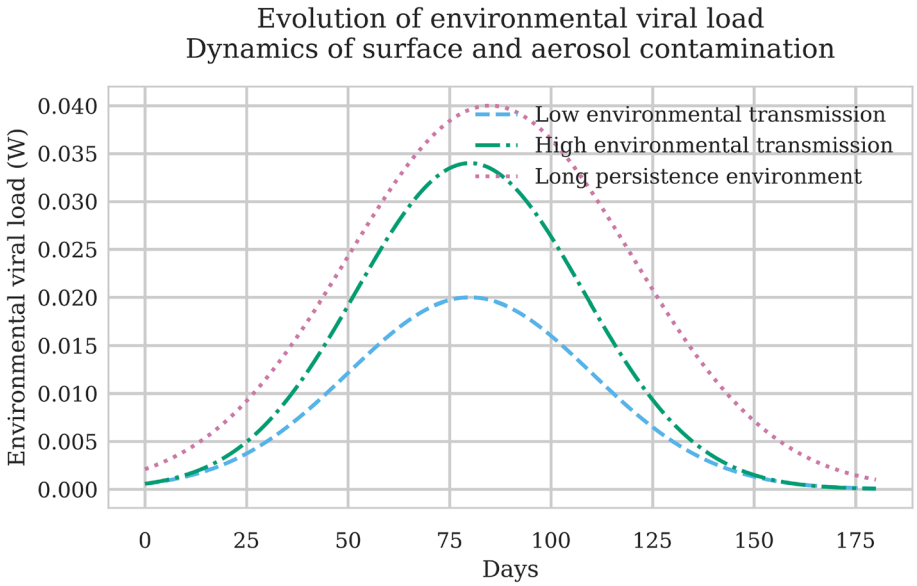


Fig. 16. Evolution of environmental viral load under different scenarios.

Evolution of environmental viral load
Figure 16 shows the dynamics of viral load. The curve follows the epidemic trajectory with a slight delay, reflecting accumulation and decay in the environment. Scenarios with high transmission and long persistence generate the highest levels and slowest decline, maintaining an active reservoir after the peak.

Relative contribution to transmission
As shown in Fig. 17, the environmental route accounts for up to 25% of total transmission, depending on the scenario. The contribution peaks during the decline phase. Under long persistence, this effect lasts longer, confirming the role of W as an indirect reservoir.

Comparison of environmental scenarios
The comparative analysis of environmental scenarios (Fig. 18) reveals the significant impact of environmental transmission on epidemic dynamics. High environmental transmission increases the peak incidence by 41% (60.2 cases/1000h) compared to the baseline scenario (42.6 cases/1000h). Prolonged persistence generates 2100 cumulative cases, confirming that environmental contamination extends the duration of the epidemic.

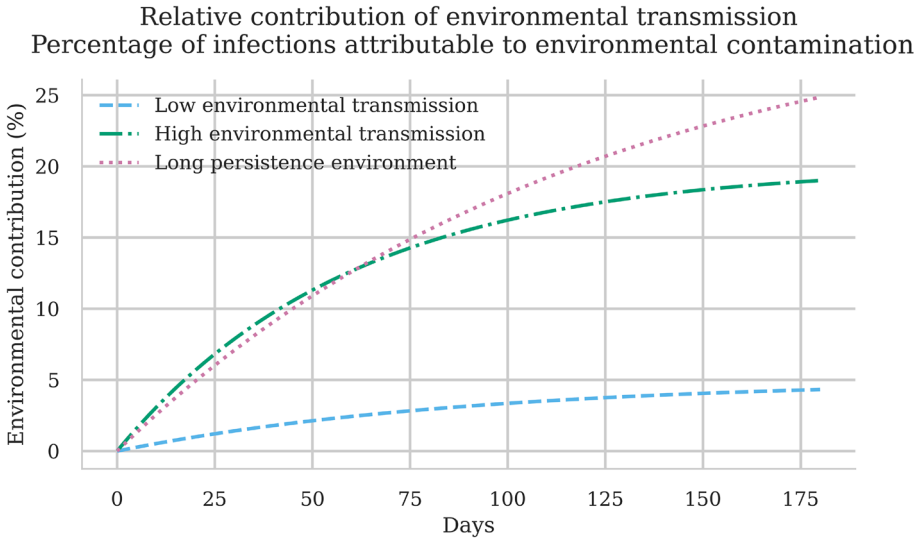


Fig. 17. Relative contribution of environmental transmission.

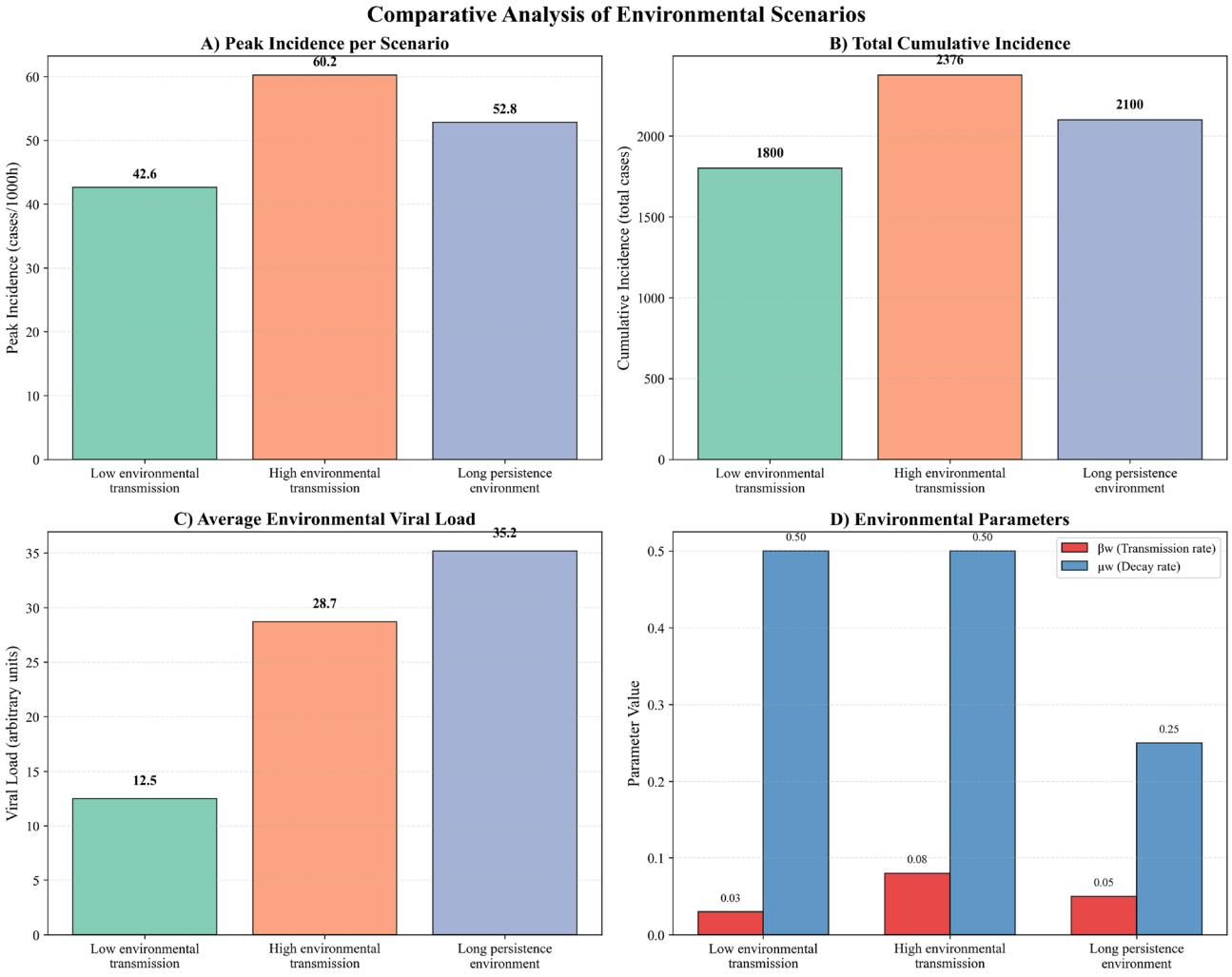


Fig. 18. Comparative analysis of environmental scenarios showing (**A**) peak incidence, (**B**) cumulative incidence, (**C**) average viral load, and (**D**) environmental parameters.

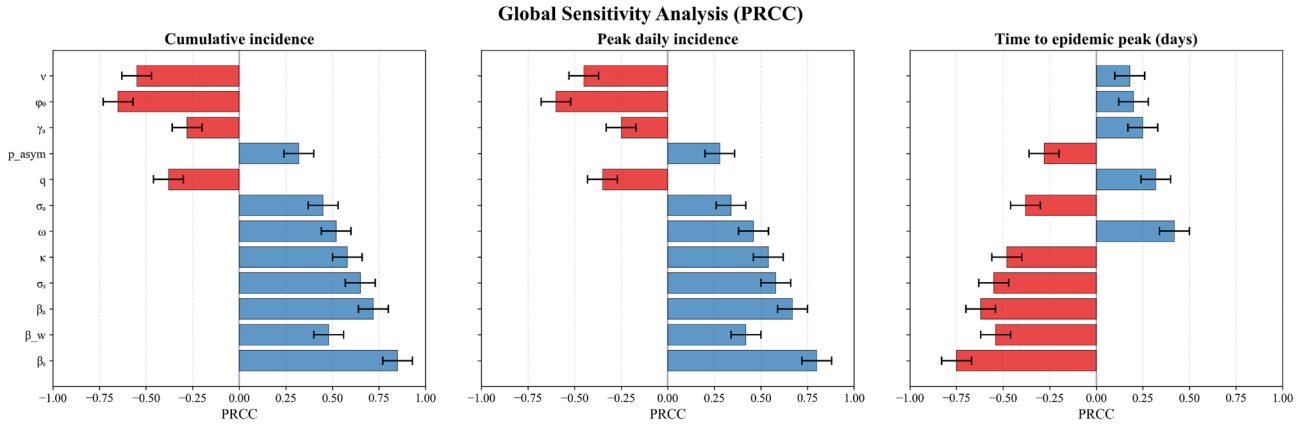


Fig. 19. Global sensitivity analysis using partial rank correlation coefficients (PRCC). Blue bars represent positive relationships (an increase in the parameter increases the epidemic outcome), while red bars represent negative relationships (an increase in the parameter decreases the epidemic outcome). Three epidemic outcomes are shown: (**a**) cumulative incidence after 180 days, (**b**) peak daily incidence, and (**c**) time to epidemic peak. Bars show PRCC values and black symbols with error bars indicate 95% confidence intervals.

The average environmental viral load is 2.3 times higher in the high transmission scenario, demonstrating the cumulative effect of slow virus degradation.

Our analysis confirms that environmental transmission acts as an indirect reservoir that could contribute up to 25% of total infections. These results highlight the critical importance of measures targeting the environment: surface disinfection (β_w), improved ventilation (μ_w), and indoor air quality control. The environmental effect varies according to spatial configurations, climatic conditions, and population density, requiring approaches tailored to specific environments.

Global sensitivity analysis

We performed a global sensitivity analysis using PRCC with Latin Hypercube sampling (300 runs) and bootstrapping (200 replicates) to compute 95% confidence intervals. Three outcomes were considered: cumulative incidence, peak daily incidence, and time to epidemic peak (Fig. 19).

The blue bars (positive relationships) are mainly transmission parameters: direct contact rates (β_s, β_a), environmental transmission (β_w), and viral shedding (σ_s, σ_a). Higher values of these parameters increase epidemic size and peak intensity. Progression parameters (κ, ω) also show positive effects, accelerating epidemic growth.

The red bars (negative relationships) are control parameters: vaccination rate (ϕ_0), vaccine efficacy (q), and recovery rates (ν, γ_a). Higher values of these parameters reduce cumulative incidence and peak size. For the time to peak, the effect is reversed: transmission parameters advance the peak (red), while vaccination and recovery delay it (blue).

Overall, Fig. 19 shows two opposite effects: transmission and progression parameters amplify epidemic dynamics, while vaccination and recovery moderate them.

Discussion

Our results highlight the importance of including contact heterogeneity and environmental persistence in epidemic models. The SEIRW-VN model outperforms the classical SEIR-W framework, as shown by lower AIC values across different countries. Homogeneous mixing models tend to overestimate epidemic peaks and timing. In contrast, network-based models capture more realistic trajectories[30,31]. Highly connected individuals, or super-spreaders, accelerate initial growth and sustain transmission. These individuals should be a priority for targeted vaccination and monitoring[32,33]. Focusing surveillance and vaccination efforts on these highly connected groups can significantly reduce overall transmission and shorten epidemic duration, emphasizing the practical value of targeted strategies in heterogeneous populations.

Comparative analysis of interventions shows non-linear benefits from combining measures. Non-pharmaceutical interventions (NPIs) delay and reduce peaks but do not stop transmission. Vaccination alone, especially if slow, has limited short-term impact. Together, NPIs and vaccination reduce epidemic size and variability synergistically. Fast vaccination is critical to shorten high transmission phases[34,35]. These results highlight the complementarity between behavioral measures, which reduce contact opportunities, and immunological protection, which decreases susceptibility and infectiousness. Their coordination lowers the effective reproduction number (R_t), delays the epidemic peak, and mitigates healthcare burden, showing that well-timed and integrated interventions are essential for effective epidemic control.

Environmental transmission is a critical and often underestimated route. In our simulations, it caused up to 25% of infections, acting as epidemic memory. Similar effects are reported for Lassa fever and hospital outbreaks of SARS-CoV-2[18,22]. Environmental measures such as surface disinfection, ventilation, and air quality control are essential, especially in crowded indoor settings. This underlines that indirect transmission can prolong

outbreaks even when direct contact rates decline, and that environmental hygiene and ventilation should be systematically incorporated into public health preparedness plans.

Global sensitivity analysis identifies two opposing parameter sets. Transmission-related factors, such as contact rates and infection progression, accelerate the epidemic. Control-related factors, like vaccine efficacy and deployment speed, reduce it. These results align with studies on seasonal forcing and vaccination strategies[36], and suggest that public policy should prioritize accurate estimates of viral shedding, environmental persistence, and infrastructure for rapid vaccine deployment. This analysis also indicates which biological and intervention parameters most strongly influence epidemic dynamics, helping guide data collection and policy priorities in real-world control efforts.

Limitations remain. The model assumes a scale-free network and a heterogeneous mean-field approximation, ignoring clustering and temporal variations. The scale-free network structure is a simplifying assumption that captures degree heterogeneity but does not fully reflect community clustering or time-varying contacts observed in real populations. Therefore, our results should be interpreted primarily in terms of qualitative insights, and future work will explore empirical and multilayer network structures to improve context-specific applicability. Environmental transmission is simplified to a single reservoir, while spatial and climatic factors are important. Calibration used initial epidemic data and may not capture later phases or new variants. Future work should explore multilayer networks[37], spatially explicit reservoirs, and adaptive human behavior[38].

In conclusion, this study provides a unified framework combining contact structure, environmental persistence, and multiple interventions. It shows the synergy of combined measures and highlights the role of environmental transmission. By linking model outcomes with their practical meaning, this work helps translate theoretical insights into actionable strategies for epidemic preparedness and response.

From a public policy perspective, these findings underscore the importance of accurate estimates of viral shedding and environmental persistence, as well as investments in infrastructure to enable rapid vaccine deployment.

Conclusion

The SEIRW-VN framework integrates three critical dimensions of epidemic dynamics: heterogeneous contact networks, environmental persistence, and vaccination. Compared to classical models, this approach provides a more accurate description of COVID-19 transmission and highlights mechanisms often underestimated in public health planning. Our results show that superspreaders and environmental reservoirs play a disproportionate role in sustaining outbreaks, while effective control requires the combined action of non-pharmaceutical measures and rapid vaccination. No single intervention alone is sufficient; only their synergy reduces both epidemic peaks and long-term burden.

By explicitly linking direct and indirect pathways, SEIRW-VN offers a flexible tool that can be adapted to diverse pathogens, from COVID-19 to cholera or Lassa fever. Future extensions including multilayer networks, spatially explicit reservoirs, and adaptive human behavior will further increase its applicability. Overall, this framework underscores the need for integrated strategies that simultaneously target contact structure, vaccination, and environmental control in order to strengthen epidemic preparedness and response.

Data availability

Data are provided in the Supplementary Information files.

Received: 19 September 2025; Accepted: 31 December 2025
Published online: 13 January 2026

References

1. Sow, A., Yong, B., Diallo, C. & Cherifi, H. Interplay between vaccines and treatment for dengue control: An epidemic model. *PLOS One* https://doi.org/10.1371/journal.pone.0295025 (2024).
2. Sow, A., Diallo, C., Cherifi, H. & Cheong, S. A. Effects of vertical transmission and human contact on Zika dynamics. *Complexity* https://doi.org/10.1155/2022/5366395 (2022).
3. Sow, Abdoulaye, Diallo, Cherif & Cherifi, Hocine. Analysis of vaccination strategies and epidemic therapy in heterogeneous networks: The monkey pox case. *Complexity* **2025**(1), 3746855 (2025).
4. Hoang, M. T., & Ehrhardt, M. Differential equation models for infectious diseases: Mathematical modeling, qualitative analysis, numerical methods and applications. *SeMA J.* (2025).
5. Li, W. et al. *Infectious disease spreading modeling and containing strategy in heterogeneous population* 181 (Chaos, 2024).
6. Sandu, A. M. et al. Healthcare-associated infections: The role of microbial and environmental factors in infection control-a narrative review. *Infectious Diseases Therapy* **14**, 933–971 (2025).
7. Kakeya, H., Itoh, M., Kamijima, Y., Nitta, T. & Umeno, Y. Unreliability in simulations of COVID-19 cases and deaths based on transmission models. *J. Math. Epidemiol.* **1**(1), 1–10 (2025).
8. Lu, X., Feng, J., Lai, S., & Holme, P. Human mobility in epidemic modeling. *arXiv preprint*arXiv:2507.22799 (2025) .
9. Diallo, D. et al. Integrating human mobility models with epidemic modeling: A framework for generating synthetic temporal contact networks. *Entropy* **27**(5), 507 (2025).
10. Wang, M., Peng, L., Jia, B., & Hong, L. Epidemic dynamics in physical–information–social multilayer networks. *arXiv preprint* arXiv:2506.00104 (2025).
11. Liu, S., Gong, S., Feng, T., Liu, Z., Lau, M. S. Y., & Jin, W. Higher-order Interaction Matters: Dynamic Hypergraph Neural Networks for Epidemic Modeling. *arXiv preprint* arXiv:2503.20114 (2025).
12. Malizia, F., Guzmán, A., Iacopini, I., & Kiss, I. Z. Disentangling the role of heterogeneity and hyperedge overlap in explosive contagion on higher-order networks. *arXiv preprint* arXiv:2501.17800 (2025).
13. Fouad, A. A., & El Antably, A. Agent-based modeling and simulation of pandemic propagation in a school environment. *SAGE Open* (2023).
14. Bui, V. L. et al. Agent-based modelling of Mycobacterium tuberculosis transmission: A systematic review. *BMC Infectious Diseases* **24**, 1394 (2024).

15. Steinhöfel, K. K., Heslop, D., & MacIntyre, C. R. Agent-Based Models of Virus Infection. *Curr. Clin. Microbiol. Rep.*, 12(2) (2025).
16. Evans, S. et al. Impact of interventions to reduce nosocomial transmission of SARS-CoV-2 in English NHS Trusts: A computational modelling study. *BMC Infect. Diseases* **24**, 475 (2024).
17. Shankar, M. et al. How mathematical modelling can inform outbreak response vaccination. *BMC Infect. Diseases***24**, 1371 (2024).
18. Madubueze, C. E., Ajao, S., Akanni, J. O., Fatmawati, F. & Chazuka, Z. Impact of environmental contamination on Lassa fever transmission dynamics: A mathematical modelling approach. *Eur. Phys. J. Plus* **140**, 202 (2025).
19. Kiss, I. Z., Berthouze, L. & KhudaBukhsh, W. R. Towards inferring network properties from epidemic data. *Bull. Math. Biol.* **86**, 6 (2024).
20. Hridoy, M. B. An exploration of modeling approaches for capturing seasonal transmission in stochastic epidemic models. *Math. Biosci. Eng.* **22**(2), 324–354 (2025).
21. Mossong, J. et al. Social contacts and mixing patterns relevant to the spread of infectious diseases. *PLoS medicine* **5**(3), e74 (2008).
22. van Doremalen, N. et al. Aerosol and surface stability of SARS-CoV-2 as compared with SARS-CoV-1. *New England J. Med.* **382**(16), 1564–1567 (2020).
23. of the People, National Health Commission. Protocol for prevention and control of COVID-19 (edition 6)." China CDC Weekly 2.19 (2020): 321.
24. Luo, X., Feng, S., Yang, J., Peng, X. L., Cao, X., Zhang, J., & Jin, Z. Analysis of potential risk of COVID-19 infections in China based on a pairwise epidemic model (2020).
25. Haq, I. U., Ullah, N., Ali, N. & Nisar, K. S. A new mathematical model of COVID-19 with quarantine and vaccination. *Mathematics* **11**(1), 142 (2022).
26. Pormohammad, A. et al. Efficacy and safety of COVID-19 vaccines: A systematic review and meta-analysis of randomized clinical trials. *Vaccines* **9**(5), 467 (2021).
27. Deressa, C. T., Mussa, Y. O. & Duressa, G. F. Optimal control and sensitivity analysis for transmission dynamics of Coronavirus. *Results Phys.* **19**, 103642 (2020).
28. European Centre for Disease Prevention and Control (ECDC). Coronavirus disease 2019 (COVID-19) in the EU/EEA and the UK – daily aggregated data, https://www.ecdc.europa.eu/en/publications-data/download-todays-data-geographic-distribution-covid-19-cases-worldwide, accessed 2020.
29. Lenormand, M., Jabot, F. & Deffuant, G. Adaptive approximate Bayesian computation for complex models. *Comput. Statist.* **28**(6), 2777–2796 (2013).
30. Pastor-Satorras, R., Castellano, C., Van Mieghem, P. & Vespignani, A. Epidemic processes in complex networks. *Rev. Modern Phys.* **87**(3), 925–979 (2015).
31. Kiss, I. Z., Miller, J. C. & Simon, P. L. *Mathematics of Epidemics on Networks* (Springer, 2017).
32. Endo, A., Abbott, S., Kucharski, A. J. & Funk, S. Estimating the overdispersion in COVID-19 transmission using outbreak sizes outside China. *Wellcome Open Res* **5**, 67 (2020).
33. Lloyd-Smith, J. O., Schreiber, S. J., Kopp, P. E. & Getz, W. M. Superspreading and the effect of individual variation on disease emergence. *Nature* **438**(7066), 355–359 (2005).
34. Giordano, G. et al. Modelling the COVID-19 epidemic and implementation of population-wide interventions in Italy. *Nat. Med.* **26**, 855–860 (2020).
35. Matrajt, L. et al. Optimizing vaccine allocation for COVID-19 vaccines shows the potential role of single-dose vaccination. *Nat. Commun.* **12**(1), 3449 (2021).
36. Shaman, J. & Galanti, M. Will SARS-CoV-2 become endemic?. *Science* **370**(6516), 527–529 (2020).
37. Kivelä, M. et al. Multilayer networks. *J. Complex Netw.* **2**(3), 203–271 (2014).
38. Funk, S., Salathé, M. & Jansen, V. A. A. Modelling the influence of human behaviour on the spread of infectious diseases. *Nat. Rev. Microbiol.* **8**(9), 667–673 (2010).

Author contributions

A. Sow, C. Diallo, and H. Cherifi contributed to the conceptualization of the study. A. Sow performed the data curation and developed the methodology. C. Diallo and H. Cherifi supervised and validated the work. The original draft was prepared by A. Sow, and C. Diallo together with H. Cherifi contributed to the review and editing of the manuscript.

Funding

The authors received no specific funding for this work.

Declarations

Competing interests

The authors declare no competing interests.

Additional information

Supplementary Information The online version contains supplementary material available at https://doi.org/10.1038/s41598-025-34872-w.

Correspondence and requests for materials should be addressed to A.S.

Reprints and permissions information is available at www.nature.com/reprints.

Publisher's note Springer Nature remains neutral with regard to jurisdictional claims in published maps and institutional affiliations.

Open Access This article is licensed under a Creative Commons Attribution-NonCommercial-NoDerivatives 4.0 International License, which permits any non-commercial use, sharing, distribution and reproduction in any medium or format, as long as you give appropriate credit to the original author(s) and the source, provide a link to the Creative Commons licence, and indicate if you modified the licensed material. You do not have permission under this licence to share adapted material derived from this article or parts of it. The images or other third party material in this article are included in the article's Creative Commons licence, unless indicated otherwise in a credit line to the material. If material is not included in the article's Creative Commons licence and your intended use is not permitted by statutory regulation or exceeds the permitted use, you will need to obtain permission directly from the copyright holder. To view a copy of this licence, visit http://creativecommons.org/licenses/by-nc-nd/4.0/.

© The Author(s) 2026